Phase synchronization in the two-dimensional Kuramoto model: Vortices and duality

Mrinal Sarkar[*] and Neelima Gupte[†]

Department of Physics, Indian Institute of Technology Madras, Chennai 600036, India

We study a system of Kuramoto oscillators arranged on a two-dimensional periodic lattice where the oscillators interact with their nearest neighbors, and all oscillators have the same natural frequency. The initial phases of the oscillators are chosen to be distributed uniformly between $(-\pi, \pi]$. During the relaxation process to the final stationary phase, we observe different features in the phase field of the oscillators: initially, the state is randomly oriented, then clusters form. As time evolves, the size of the clusters increases and vortices that constitute topological defects in the phase field form in the system. These defects, being topological, annihilate in pairs; i.e., a given defect annihilates if it encounters another defect with opposite polarity. Finally, the system ends up either in a completely phase synchronized state in case of complete annihilation or a metastable phase locked state characterized by presence of vortices and antivortices. The basin volumes of the two scenarios are estimated. Finally, we carry out a duality transformation similar to that carried out for the *XY* model of planar spins on the Hamiltonian version of the Kuramoto model to expose the underlying vortex structure.

I. INTRODUCTION

The phenomenon of collective synchronization is one of the most fascinating phenomena observed in nature [1,2] as well as in many branches of science, such as biological, physical, chemical, and social sciences. A few typical examples of collective synchronization include the rhythmic applause of an audience, the chirping of crickets, the flashing of fireflies, the synchronized firings of coupled neurons, and the coordinated conduction of the heart's pacemaker cells [3] seen in biological and social sciences. Synchronization can also be seen in experimental systems such as arrays of Josephson junctions [4], laser arrays [5,6], etc., in physics. The Kuramoto model is a paradigmatic model to study synchronization in such many-body interacting systems. The original model consists of a population of oscillators where each oscillator is coupled to all others with the same strength and their natural frequencies are drawn from a given frequency distribution. This model with mean-field coupling, being simple and analytically tractable, has been studied in great detail for a long time [7–10]. It exhibits a transition from an incoherent state to a coherent state as the coupling strength varies. The critical coupling value, beyond which the system starts to synchronize depends on the frequency distribution. A phase transition is seen from a desynchronized phase at low coupling-strengths to collective synchronization at high coupling-strengths. Although the mean-field version of the model has found many applications in different contexts; many variants with other kinds of coupling have been found to be useful in various contexts. Hence, many examples, such as the Kuramoto model with local coupling [11–18], the Kuramoto model with frustration [19–22],

Kuramoto model with time-delayed coupling [23–25], Kuramoto oscillators based on different types of graphs [26–28], etc., have also been studied over the years. Here, we consider one such variation, where the oscillators based on a 2-d lattice interact locally, with their nearest neighbors only.

Previous studies on locally coupled Kuramoto models focused mainly on their stationary state dynamics. The possibility of phase transitions in such models was investigated. Strogatz *et al.* [12] calculated the probability of phase-locking in such locally coupled systems. This probability tends to zero in the thermodynamic limit, i.e., there can not be any entrainment transition in locally coupled system in the thermodynamic limit. In fact, this is true for any spatial dimensionality. However, in finite systems, the dynamics exhibits a crossover from desynchronization to synchronization as the coupling strength varies. Hong *et al.* [17] studied the possibility of a phase transition for the full nonlinear system in different spatial dimensions including two-dimensional (2D) systems. Lee *et al.* [18] analyzed the transition for oscillators in a two-dimensional lattice via the stability of vortex-antivortex pairs formed in the phase-field of the oscillators. Moreover, they also showed that the critical coupling-strength (K_c) depends on system-size (N) as $K_c \sim \log(N)$ as long as system-size is small. However, there have been no detailed studies of its relaxation dynamics.

Here, in this communication, we consider a system of Kuramoto oscillators based on a two-dimensional square lattice with nearest-neighbor interactions and study its relaxation dynamics. The manner in which a system of globally coupled oscillators with distributed natural frequencies relaxes to the steady state from an initial incoherent state has been studied earlier [20,29–32]. During relaxation, metastable states are found in some systems which are due to finite-size effects [31]. In some oscillator models, there may exist synchronized glassy phases [20,32]. Such systems are characterized

─────────
*mrinal@physics.iitm.ac.in
†gupte@physics.iitm.ac.in

by their slow relaxation dynamics. Moreover, relaxation dynamics also shows how a a system recovers its own stationary dynamics once it gets perturbed from the stationary state.

In our present study, we choose the oscillators to be identical. This system of identical oscillators, being locally coupled, admits a number of fixed point solutions and reaches different stationary states. We call these states "metastable states," as these states are long lived and clearly represent local minima in the interaction potential. The system can relax to different metastable states depending on initial conditions. We start with a random initial condition drawn from a uniform distribution of phases of the oscillators and observe how the system relaxes to the stationary state. During the relaxation process, distinct configurations of the phase-field of the oscillators are observed. Initially, locally synchronized clusters are formed. As time progresses, the cluster sizes increase. At longer times, we observe the formation of vortices which are topological defects in the phase field of the oscillators. These vortices interact with each other, and play a crucial role in the eventual synchronization dynamics of the system.

We found that the stationary-state dynamics depends on both the system-size and the initial distribution of phases of the oscillators. Depending on the initial distribution of the phases, the final stationary state can be broadly classified in two categories, namely completely phase synchronized states and phase-locked states. The basin of attraction of these states is also studied. We observe, that the size of the basin of the completely phase synchronized states decreases as the system-size increases. Thus, the usual steady states for large system-sizes are phase-locked states, which are primarily dominated by presence of vortices and antivortices. Moreover, we also study the system-size dependency of the average relaxation time.

We attempt to uncover the underlying vortex structure in the Kuromoto phase field dynamics using the methods used for the *XY* model of statistical mechanics. For this, we need the Hamiltonian version of the model. A recent study [33] shows that a classical Hamiltonian system (in the action-angle representation) with $2N$ state variables exhibits a family of invariant tori (with homogeneous actions) on which the angle variable follows exactly the same dynamics as that of Kuramoto model. We use this Hamiltonian to calculate the canonical partition function and apply the duality transformation on this partition function to expose the underlying vortex-structures at low-temperatures.

The paper is organized as follows. In Sec. II, we describe the model explicitly and mention some of the previous results in this context. We describe the different features observed during relaxation and different stationary states in Sec. III. Next, in Sec. IV, we apply the duality transformation on the Hamiltonian to study the formation of vortices at low temperatures. Finally, in Sec. V, we summarize our results and future scope.

II. THE MODEL

We consider a system of Kuramoto oscillators based on a two-dimensional square lattice where, all the oscillators have the same natural frequency and each oscillator interacts with its nearest neighbors only. The phase evolution equation of the
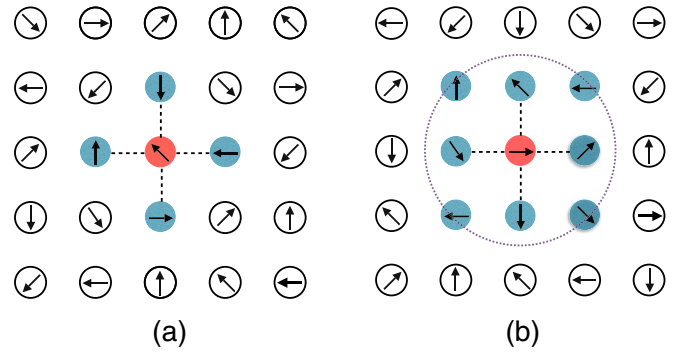

FIG. 1. A schematic diagram of a periodic array of oscillators based on a two-dimensional square lattice. (a) A diagram of the coupling scheme (diffusive coupling) in our model where each oscillator (e.g., the one indicated in red) is coupled to its nearest neighbors (indicated in blue). (b) To calculate the local order parameter of each oscillator (red), nearest neighbors and next nearest neighbors (blue) are taken into consideration.

(i, j)th oscillator is given by

$$\frac{d\theta_{i,j}}{dt} = \omega_{i,j} + K[\sin(\theta_{i+1,j} - \theta_{i,j}) + \sin(\theta_{i-1,j} - \theta_{i,j})$$
$$+ \sin(\theta_{i,j+1} - \theta_{i,j}) + \sin(\theta_{i,j-1} - \theta_{i,j})], \quad (1)$$

where $\theta_{i,j}$, $\omega_{i,j}$ are the phase and the natural frequency of the (i, j)th oscillator, respectively, and $i, j = 1, 2, 3, ..., N$. The parameter $K(> 0)$ is the coupling strength and $N \times N$ is the size of the square array. Since the oscillators have identical frequencies,

$$\omega_{i,j} = \omega \quad \forall i, j.$$

Fig. 1(a) shows a schematic diagram of the manner in which each oscillator is coupled to its neighbors. We assume periodic boundary conditions in our system.

We study complete phase synchronization in this system. Let us assume that $\{\theta_{ij}(t)\}_{i,j=1}^{N}$ is the complete set of phases for this model system [Eq. (1)]. The oscillators are said to be phase synchronized if

$$\lim_{t \to \infty} |\theta_{i,j}(t) - \theta_{l,m}(t)| = 0 \quad \text{for} \quad i, j \neq l, m \quad (2)$$

and phase-locked if

$$\lim_{t \to \infty} |\theta_{i,j}(t) - \theta_{l,m}(t)| = \text{constant} \quad \text{for} \quad i, j \neq l, m. \quad (3)$$

To quantify the degree of coherence, the global order parameter ρ for the system is defined as follows:

$$\rho = \frac{1}{M} \left| \sum_{i,j} \exp(i\theta_{i,j}) \right|,$$

where M is the total number of oscillators in the system.

Since the oscillators are identical, the evolution equations can be written as the gradient of some function, as follows:

$$\frac{\partial \theta_{i,j}}{\partial t} = -\frac{\partial}{\partial \theta_{i,j}} K[\cos(\theta_{i+1,j} - \theta_{i,j}) + \cos(\theta_{i-1,j} - \theta_{i,j})$$
$$+ \cos(\theta_{i,j+1} - \theta_{i,j}) + \cos(\theta_{i,j-1} - \theta_{i,j})]. \quad (4)$$

For a gradient system, all the stationary states correspond to the fixed points of the system. There are no limit cycles or any other kinds of attractor. We note that distinct initial configurations of the phases can lead to distinct fixed points for any given value of the coupling constant. Thus, for any stationary state, the fixed point condition gives

$$\frac{d\theta_{i,j}^{st}}{dt} = 0, \quad \forall\, i,j$$
$$\Rightarrow K[\sin(\theta_{i+1,j} - \theta_{i,j}) + \sin(\theta_{i-1,j} - \theta_{i,j})$$
$$+ \sin(\theta_{i,j+1} - \theta_{i,j}) + \sin(\theta_{i,j-1} - \theta_{i,j})] = 0 \quad (5)$$

(for the choice, $\omega = 0$). The solutions to the above equation [Eq. (5)] can be of two types:

(1) All oscillators have the same phase, i.e., $\theta_{i,j}^{st} = \theta_0$(constant) $\forall\, i,j$, which is essentially the state of complete phase synchronization.

(2) Oscillator phases are constant in time but their values are different from each other satisfying the condition [Eq. (5)]. This corresponds to phase-locked solutions.

When the initial configuration of the oscillators has phases which are distributed randomly following a uniform distribution, during their evolution following the governing dynamics [Eq. (1)], they may either get phase locked or completely phase-synchronized. We note also that many distinct solutions of the phase locked type are possible corresponding to many distinct fixed points for the system each with its own basin of attraction. The system evolves to a given fixed point provided the initial condition for evolution lies in the basin of attraction of that fixed point. It is therefore pertinent to identify the fixed points or equilibrium states of the system, and also to study the modes of relaxation to these states. For this, the evolution is initiated with different random initial configurations for the phases of the oscillators and the system is evolved for a sufficiently long time for the order parameter to settle down to some value. Figure 7(a) indicates how the global order parameter value changes as the system of finite size ($N = 50 \times 50$) relaxes to equilibrium for a particular value of coupling strength for different initial conditions. Depending on initial conditions, the system ends up in different phase-locked states or completely phase-synchronized states.

Here, the relaxation dynamics of the system is studied numerically using the fourth order Runge-Kutta method with step size 0.02. The initial distribution of phases was uniformly random distributed over the range $(-\pi, +\pi]$. In the next section the relaxation dynamics is described for the value $K = 1.0$ for the coupling constant. However, we note that the relaxation dynamics is the same for all values of K due to the following rescaling argument.

The evolution equation [Eq. (1)], after a rescaling of time and frequency via the equations $t' = Kt$ and $\omega' = \omega/K$, will read

$$\frac{d\theta_{i,j}}{dt'} = \omega' + [\sin(\theta_{i+1,j} - \theta_{i,j}) + \sin(\theta_{i-1,j} - \theta_{i,j})$$
$$+ \sin(\theta_{i,j+1} - \theta_{i,j}) + \sin(\theta_{i,j-1} - \theta_{i,j})]. \quad (6)$$

Thus, K can be set equal to unity by the rescaling above. Hence, it is sufficient to study the dynamics for the $K = 1$ case. Further, in this study, we have set the value of the frequency, which is identical for all oscillators, to zero, which

can always be done by choosing a frame of reference rotating with that identical frequency ω. We note that the synchronized state is reached earlier for higher values of K, and different stages in the dynamics will occur at earlier times for this case.

III. RELAXATION DYNAMICS

In this section, we study the relaxation dynamics of the system, by observing the time evolution of the global order parameter ρ as well as the phase structures during this relaxation process. Initially, locally synchronized clusters are formed. As time progresses, we observe spin waves and vortices in the phase field of the oscillators. These vortices and antivortices move in time and as soon as any two vortices of opposite polarity meet, they annihilate. Whenever there is annihilation, there is a clear jump in the ρ value. The vortex annihilation process continues till the system reaches equilibrium. The equilibrium state may be reached after a complete annihilation of vortex pairs, or may still have some vortex pairs left, depending on initial conditions. For some initial conditions, there is complete annihilation of the defects resulting in completely phase-synchronized states. Otherwise, the system reaches a phase-locked state. The phase maps at different times corresponding to complete phase synchronization for one particular choice of initial condition are shown in Fig. 2.

The qualitative nature of the overall dynamics of the phase structures is the same for all initial conditions in the beginning; however, completely phase synchronized states are reached asymptotically for only a fraction of initial conditions. We note here that the states called the asymptotic states here are long lived. In terms of simulation times, these are stationary for 4×10^6 time steps with a Runge-Kutta time step of 0.02. Several different dynamical states are observed in the relaxation dynamics. These are as follows:

A. Clusters

Initially, we observe locally synchronized clusters in the phase field of the system. As time progresses, the cluster size increases. To investigate the formation of locally synchronized clusters, a local order parameter λ is defined as follows:

$$\lambda_{ij} = \frac{1}{N_n} \left| \sum_{l,m} \exp(i\theta_{lm}) \right|,$$

where N_n is the number of nearest and next nearest neighbors [Fig. 1(b)], and l, m run over the nearest neighbors, and next nearest neighbors of the site (i, j), i.e., $(i, j+1)$, $(i, j-1)$, $(i+1, j)$, $(i-1, j)$ and $(i-1, j-1)$, $(i-1, j+1)$, $(i+1, j-1)$, $(i+1, j+1)$ (see Fig. 2). If an oscillator θ_{ij} is within a synchronized cluster, then λ_{ij} will be nearly 1. If there is a local phase singularity in the phase field, near (i, j), then $\lambda_{i,j}$ takes a very small value. Thus, the value of $\lambda_{i,j}$ gives a measure of the local degree of synchronization of the oscillators in the neighborhood of the site (i, j). Using the local order parameter map we can also identify the location of the vortices, as will be seen in the next subsection. The formation of clusters at short times is clear from the phase map, the local-order parameter map and also from the phase-field as can be seen in Figs. 2(a), 2(e), and 2(i), respectively, for a synchronized initial condition; and
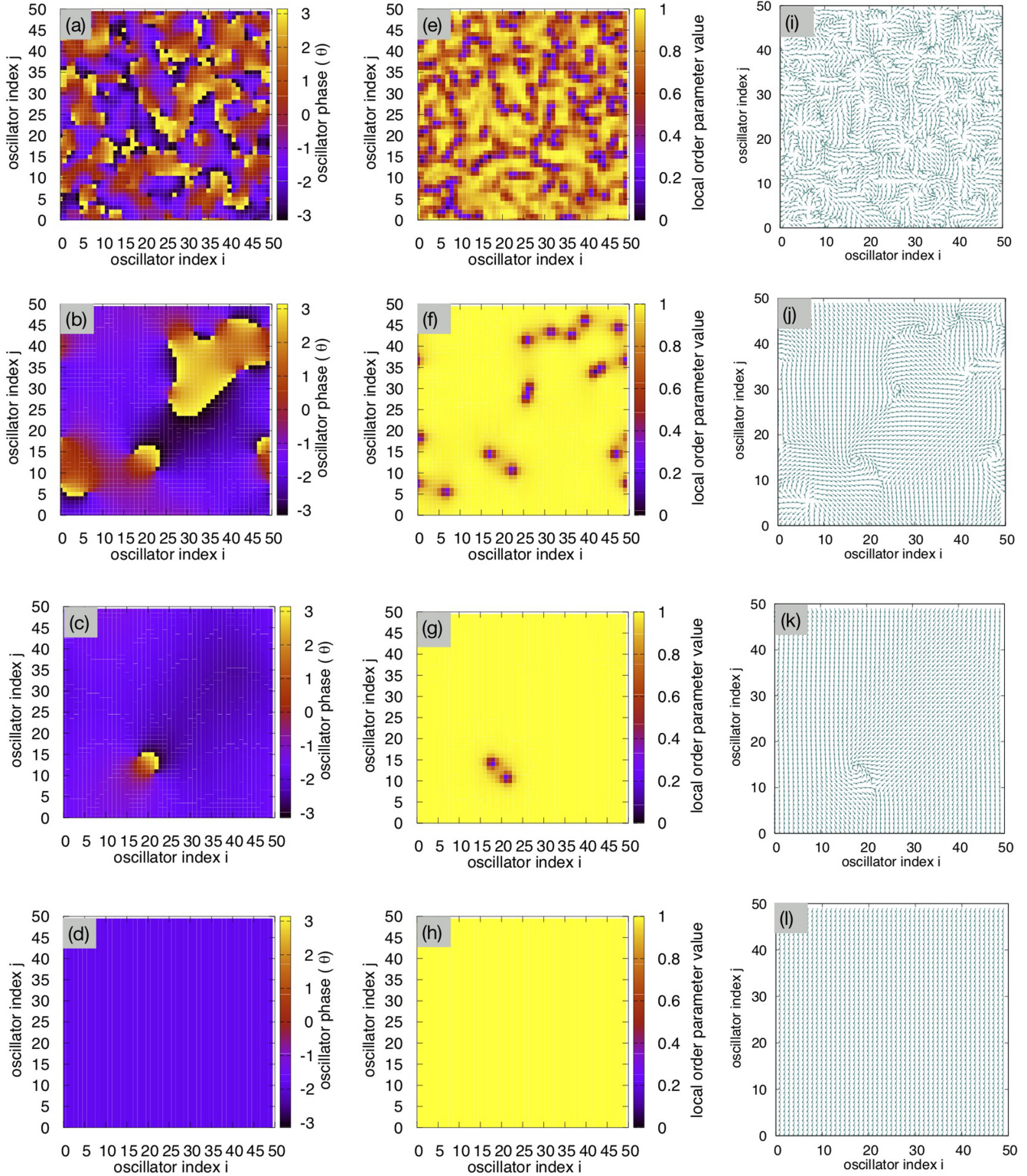
FIG. 2. In this figure, the phase-maps (a) → (d), local order parameter maps (e) → (h) and the phase-fields (i) → (l) of the system are shown at different times during relaxation for lattice size $N = 50 \times 50$ [(a), (e), (i) $t = 80$ time units, (b), (f), (j) $t = 2400$ t.u., (c), (g), (k) $t = 1 \times 10^4$ t.u., and (d), (h), (l) $t = 5 \times 10^4$ t.u.]. All of these are obtained starting from a particular initial condition for coupling strength $K = 1.0$. We set the intrinsic frequency of the oscillators to be zero. Phase-map (a) → (d): Each pixel represents one oscillator and the color indicates its phase, where $-\pi$ is represented by black while $+\pi$ is by yellow. The local order parameter map (e) → (h): Each pixel represents one oscillator and the color indicates its local order parameter value which can take any value between 0 and 1, with 0 being represented by black while 1 is indicated by yellow. This quantity indicates the local degree of synchronization of each of the oscillators. Phase-fields (i) → (l): Each arrow represents one oscillator and the direction is drawn depending on its phase.
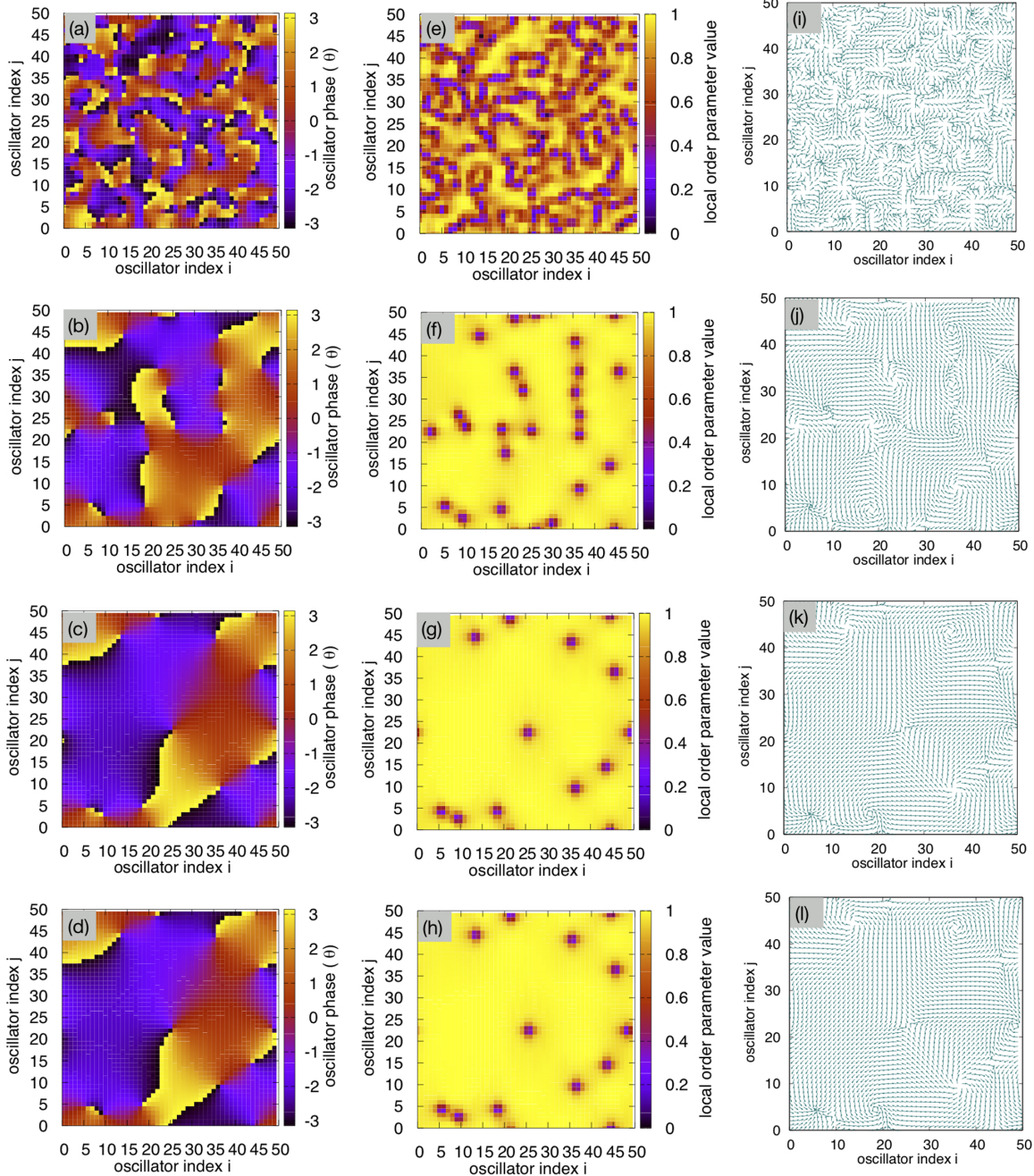
FIG. 3. Phase-maps (a) → (d), the local order parameter map (e) → (h), and Phase fields (i) → (l) are shown at different times during relaxation for lattice size $N = 50 \times 50$ [(a), (e), (i) $t = 80$ time units, (b), (f), (j) $t = 2400$ t.u., (c), (g), (k) $t = 2 \times 10^4$ t.u., (d), (h), (l) $t = 5 \times 10^4$ t.u.]. All of these are obtained starting from a particular initial condition for coupling strength $K = 1.0$. We set the intrinsic frequency of the oscillators to be zero. Phase-map (a) → (d): Each pixel represents one oscillator and the color indicates its phase, where $-\pi$ is represented by the color black while $+\pi$ is represented by yellow. The local order parameter map (e) → (h): Each pixel represents one oscillator and the color indicates its local order parameter value. It can take any value between 0 and 1, 0 being represented by black and 1 by yellow. This quantity indicates the local degree of synchronization of each of the oscillators. Phase fields (i) → (l): Each arrow represents one oscillator and the direction is drawn depending on its phase.

in Figs. 3(a), 3(e), and 3(i), respectively, for another initial condition leading to a phase-locked state.

B. Vortices

In course of time, along with the formation of locally synchronized clusters, structures where the phases organize in the form of vortices are also formed. These vortices appear at the boundaries between locally synchronized clusters. These are also called topological defects. These structures are topological in the sense that, starting from a random initial configuration of phases of the oscillators such a structure cannot be obtained by simply deforming the system continuously. The vorticity is defined as follows (in the continuum

limit):

$$\oint \nabla\theta(\hat{r}, t).d\hat{l} = \pm 2\pi n, \qquad (7)$$

where $d\hat{l}$ is the integration path enclosing the defect (singular point) and n is called the topological charge or vorticity. The vorticity is said to have charge $+1$ if the total change in phase around the defect is $+2\pi$ (for a vortex) and -1 if it is -2π (for an antivortex). The vortices appear in vortex-antivortex pairs, at any coupling strength, making the total vorticity zero. This is due to fact that the system is subject to periodic boundary conditions. The formation of vortices becomes very clear if we look at the vector plots, representing the orientation of phase-field corresponding to the phase maps. These are obtained in the following way: Each oscillator is treated as a vector of unit radius and its phase is represented by the angle it makes with the horizontal (the anticlockwise direction is taken as positive). If we look at the phase maps carefully, then we observe vortices as well as spin waves in the phase field of the oscillators. The phase map in Fig. 2(b) and the corresponding local-order parameter map and the phase-field in Figs. 2(f) and 2(j), respectively, show the formation of vortices in the phase-field of the oscillators. The local degree of synchronization is high at all points in the phase-field except for the singular points, which helps us to locate the position of the vortices. Another important point to notice is that the total number of such defects is even. Thus, the vortices and antivortices appear in pairs making the total vorticity zero, as expected. The same phase structures are observed for other initial conditions also, an example of which is shown in Figs. 3(b), 3(f), and 3(j).

C. Vortex annihilation and spin waves

The vortices formed in the phase-field of the oscillators are observed to move along the boundaries between the locally synchronized clusters. Since a vortex is topological, when it meets with another one with opposite polarity, they annihilate. Through the annihilation, the system reaches a steady-state where vortices and antivortices, may or may not exist, but there is no further annihilation. The complete annihilation of vortices in time can be seen from the phase-maps in Figs. 2(b) $\rightarrow$ 2(d) and the corresponding local-order parameter maps and phase-fields in Figs. 2(f) $\rightarrow$ 2(h) and Figs. 2(j) $\rightarrow$ 2(l), respectively. However, the phase-maps in Figs. 3(b) $\rightarrow$ 3(d) and the corresponding local-order parameter maps and phase-fields in Figs. 3(f) $\rightarrow$ 3(h) and Figs. 3(j) $\rightarrow$ 3(l), respectively, show an example where there is annihilation, but the steady state is reached before the complete annihilation of vortices, and a phase locked state is achieved.

In the phase field of the oscillators, we observe spin waves along with the presence of vortices. If there is complete annihilation between the vortices and antivortices, then spin waves are observed before the system reaches final steady state. With time, these spin waves get suppressed and the completely phase synchronized state emerges as the asymptotic state.

D. Routes to complete Phase-synchronization and to Phase-locking

The complete phase synchronization of the asymptotic state occurs only in the case of complete annihilation of the defects. Otherwise, the system gets phase-locked with these defects in the phase-field of the oscillators. Since the system is spatially extended, multi-attractor solutions are possible for the same values of the parameters, depending on initial conditions. Hence, the system reaches different steady states (i.e., fixed points of the evolution equations of the system) for different initial distributions of the phases of the oscillators. An example of the completely phase-synchronized state is shown in Fig. 2, whereas Fig. 3 shows a case where, starting from a completely disordered state, the system ends up in a phase-locked state.

Figure 4 shows schematically how the system relaxes to equilibrium through the formation of different features in the phase-field. We note that the two routes to the two asymptotic states have the first three steps in common. The initial disordered state organizes itself into locally synchronized clusters, which develop into spin waves and vortices. In the case of the first route, the vortices annihilate each other in vortex-antivortex pairs until only spin waves are left. The spins then synchronize with each other until the final phase synchronized state is reached. In the case of the second route, all the vortex-antivortex pairs do not annihilate each other. The asymptotic state is phase locked with both spin waves and vortices. A plot of the global order parameter as a function of time shows signatures of all the features described above. Figure 5 shows these plots for two typical initial conditions, one of which leads to a phase synchronized state [Fig. 5(a)], and another which leads to a phase locked state [Fig. 5(b)], both for a particular value of the coupling constant ($K = 1.0$). It is clear from the plot that there are three distinct time scales in the problem. The first scale can be seen in the inset of the figure. This is up to about 125 time steps, and has been called Region I. In this region, the formation of synchronized clusters is seen, as can be seen in the Figs. 2(a), and 3(a), respectively, for the time step $t = 80$ which lies in this interval. As mentioned above, these evolve into vortices and spin waves. The vortices carry topological charge and occur in pairs of opposing charge
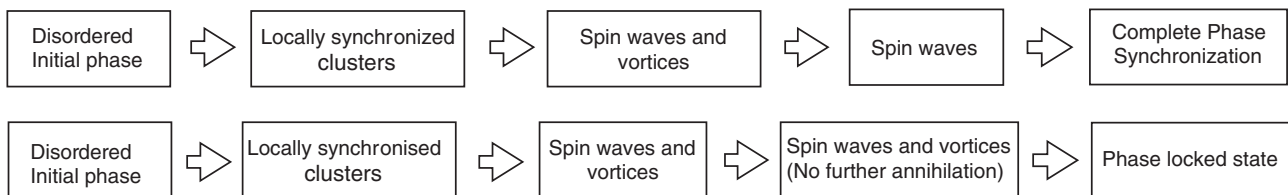

FIG. 4. A schematic diagram which shows the route by which the oscillators make a transition to either the completely phase synchronized asymptotic state (a) or a phase locked asymptotic state (b) starting from a disordered initial configuration of phases.
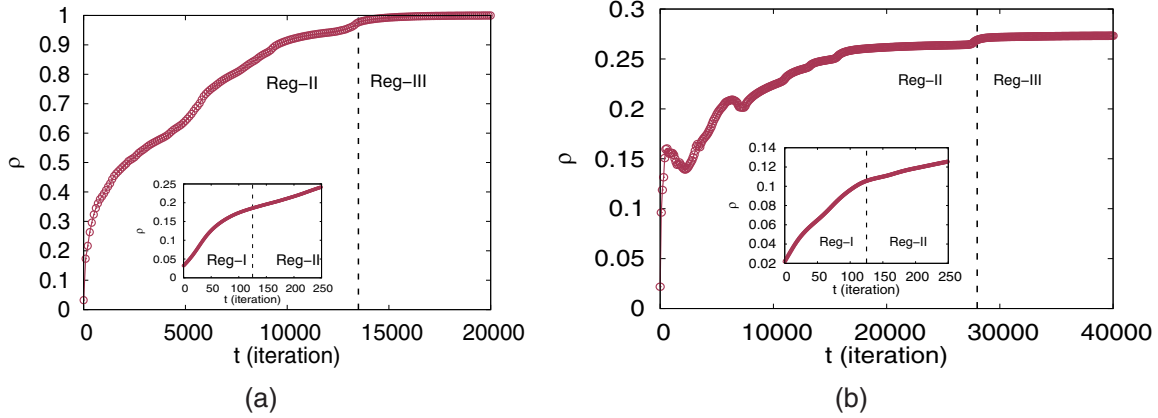
FIG. 5. Time evolution of the global order parameter is shown at coupling strength $K = 1.0$ for a system of size $N = 50 \times 50$ for two different initial conditions. Panel (a) corresponds to the initial condition leading to completely phase-synchronized state, while panel (b) corresponds to a phase-locked state. The dotted vertical lines separate the different regions in the phase-space during relaxation. We set the intrinsic frequency of the oscillators to be zero.

which move on the lattice and annihilate each other. The annihilation of vortex-antivortex pairs enhances local as well as global order and the value of the global order parameter increases steeply over the annihilation process. This is seen over the time scale labeled region-II. It can be seen that in the case of the initial condition that reaches the synchronised state, the synchronized state is reached after about 15 000 time steps. It is clear that in the case of the other initial condition that the vortex-antivortex configurations persist till the phase locked state is reached and the order parameter flattens at a value which is much less than one. The phase locked state may eventually relax to a phase synchronized state, but the phase locked state has a very long life time which depends on the system size, and is not reached during numerical simulations of length 4×10^6 Runge-Kutta time steps of step size 0.02. We discuss this further in the next subsection. We note here that the time scales noted here are K dependent, and decrease with increasing coupling. However, finite-time, finite-size studies are required for any definitive comment. These are planned elsewhere.

E. Local stability analysis of the phase-locked states

We examine the local stability of the phase locked solutions by applying a uniform perturbation of a given strength to the phase locked state. For this, the random initial conditions are allowed to settle into a phase locked state with an order parameter which is independent of time, and the phases of the oscillators are identified at some given instant. At this point, each one of these phases is perturbed by a random number $\delta\theta$ such that δ is the perturbation strength and θ lies between $(-\pi, +\pi]$. The evolution of the order parameter after the application of the perturbation is examined for several different perturbation strengths. We observe that for smaller values of perturbation, these states are locally stable, i.e., the system settles down again into a phase locked state with the same order parameter, whereas for higher values, there exists a possibility for the system to go to some other phase-locked state. Thus, the phase locked states are at least metastable states and do not evolve into the phase synchronized state within the parameters

of our simulation, or our class of random initial conditions. Figure 6 shows the evolution of the order parameter to stationary phase-locked states subject to perturbations of different strengths, $\delta = 0.1, 0.2, 0.3,$ and 0.4, with δ as defined earlier, at the time 2.5×10^5. The sudden jump in the order parameter value (as shown in the inset) at time 2.5×10^5 corresponds to the instant at which the system is perturbed and for the smaller perturbation strengths, namely $\delta = 0.1, 0.2,$ and 0.3, the system regains its previous state with time, characterized by the same order parameter value. For the higher value $\delta = 0.4$, the
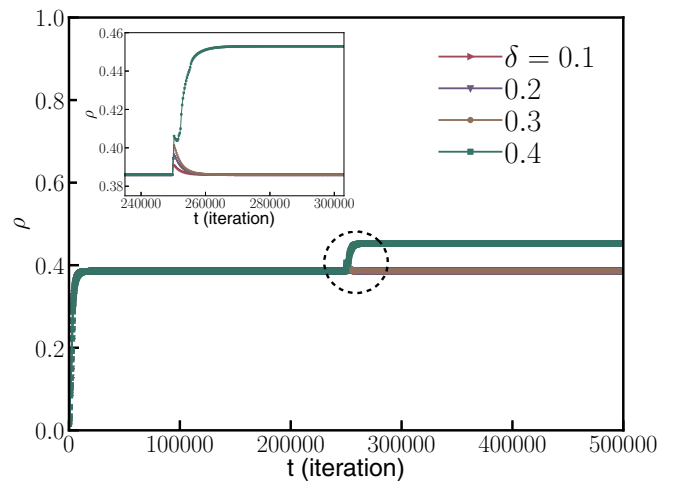

FIG. 6. The time evolution of the order parameter for system-size $N = 50 \times 50$ is shown where the final phase locked state is perturbed with various perturbation strengths, namely $\delta = 0.1, 0.2, 0.3,$ and 0.4 at time 2.5×10^5. The data is obtained by integrating the governing dynamics for $K = 1.0$. The sudden jump in the order parameter value (as shown in the inset) at the time 2.5×10^5 corresponds to the instant at which the system is perturbed and for the smaller perturbation strengths, namely $\delta = 0.1, 0.2,$ and 0.3, with time, the system regains its previous state, characterized by the same order parameter value. For $\delta = 0.4$, the system goes to another phase-locked state characterized by a different value of the order parameter value after a transient.
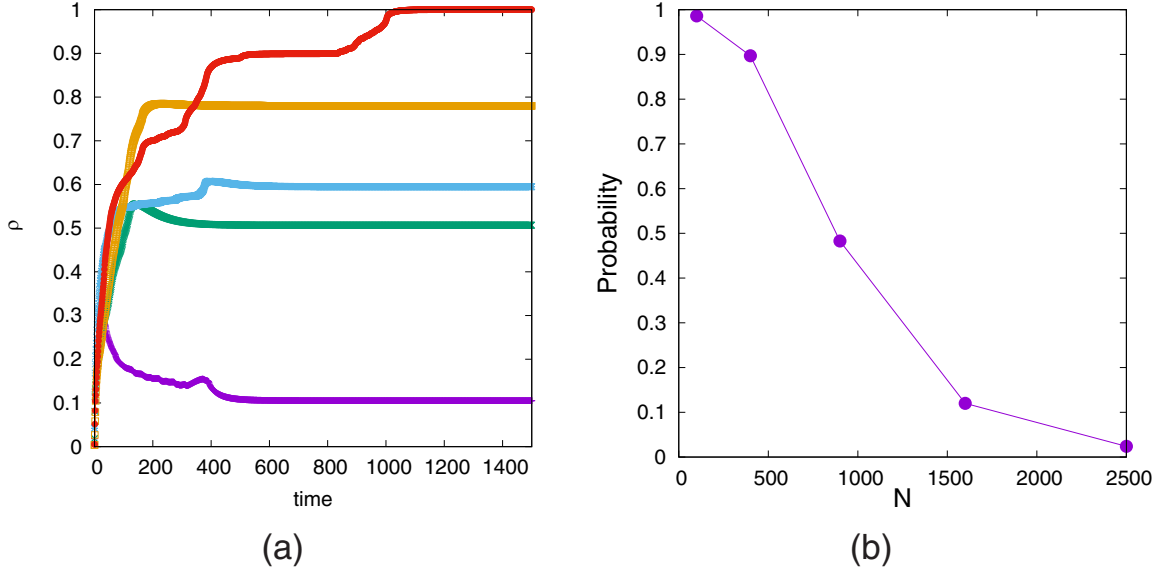
FIG. 7. Panel (a) shows the time evolution of the global order parameter for different initial conditions at coupling strength $K = 1.0$ for a system of size $N = 50 \times 50$. The fraction of initial conditions which leads to complete phase synchronization for various system-sizes is shown in panel (b). The initial phases are chosen from a uniform distribution from $(-\pi, \pi]$. We set the intrinsic frequency of the oscillators to be zero.

system goes to another phase-locked state characterized by a different time-independent order parameter value in long time. We note that the perturbation did not lead to a phase synchronized state for any of the phase locked states studied. Given this, and also given the lengths of the transient, the phase locked states appear to be quite stable. In addition, the Lyapunov spectrum contains all negative eigenvalues which also suggest that phase-locked state is locally stable.

F. Basin stability of the synchronized state

We have thus observed that the stationary states of the system can be broadly classified into two categories - phase-locked or completely phase-synchronized states. These phase-locked states are actually metastable states, characterized by presence of topological defects (vortices and antivortices). For a particular system-size, whether a stationary state would be a phase-locked or completely phase-synchronized, depends on the initial conditions. As long as the system size is small, the probability that the system reaches one of its its global minima, i.e., the completely phase synchronized states is high. This probability decreases as N increases.

We perform a simple numerical experiment with various system sizes. For each system-size, we start with 1000 initial conditions and count the number of initial conditions that lead to complete phase synchronization at large times. Here, we plot the fraction (ratio of number of initial conditions for which the system reaches its asymptotic state to the total number of initial conditions) for different system sizes. This is shown in Fig. 7(b). The fraction tends to zero as N becomes infinitely large. In other words, in the limit of large system size, the system tends to phase lock and is characterized by the presence of topological defects in the phase-field of the oscillators.

One can compute the average relaxation time, defined by $\tau_{av} = \int_0^\infty dt' \rho_{norm}(t')$ for the completely phase-synchronized states [29,34]. Here, ρ_{norm} is the normalized order parameter and is defined as: $\rho_{norm}(t) = \frac{\rho(t) - \rho_{st}}{\rho(0) - \rho_{st}}$, where ρ_{st} is order parameter value in the stationary state. At $t = 0$, $\rho_{norm} = 1$ and at saturation $(t \to \infty)$, it takes the value 0.

In our case, for a given coupling strength $(K = 1.0)$, we see indications of scaling behavior and τ_{av} increases with the linear system-size as $\tau_{av} \sim L^z$ with $z \approx 2.4$ over a small range of L values $(L < 50)$. However, since this cannot be extended to larger system sizes (e.g., $L \geqslant 100$), as for such systems, very few initial conditions reach completely phase-synchronized states. However, the approximate scaling makes it clear that the relaxation times increase faster than L^2. Hence, very long relaxation times have been observed for these systems, as seen in all the cases here.

Further, we investigate the order-parameter (ρ) of the phase-locked states for different system-sizes for the former case. The phase-locked states with larger numbers of defects correspond to lower values of ρ. We obtain the distribution of ρ for various system sizes numerically as is shown in Fig. 8. The peak of the distribution shifts towards zero as the system-size increases. We expect the order parameter value to tend to zero in the thermodynamic limit. In such a case, the behavior of the system is expected to be governed by the presence of the vortices in the phase-field of the oscillators.

We note that the stationary states depend on the initial distribution of the phases of the oscillators. Here, we have used a uniform distribution. Other types of initial conditions, e.g., a biased distribution, may lead to completely different behaviours.

We note that vortices have been observed earlier in Kuramoto oscillator systems [18], where a system of 2D Kuramoto oscillators with frequencies drawn from a Gaussian intrinsic frequency distribution is studied. The vortices
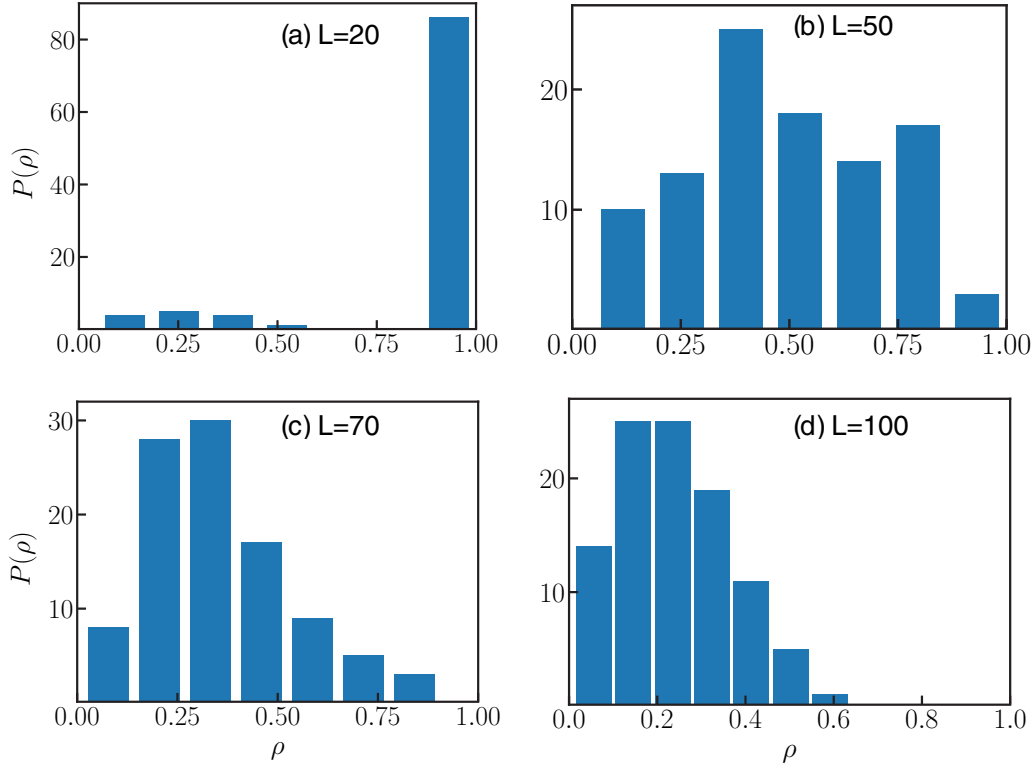
FIG. 8. $P(\rho)$, the discrete distribution of the order parameter ρ in the stationary state, is shown in the form of histogram for system-sizes (a) $N = 20 \times 20$, (b) 50×50, (c) 70×70, and (d) 100×100, respectively. The peak of the distribution tends towards zero as the system-size increases indicating vanishing of ρ in the thermodynamic limit. For each system-size, this distribution is obtained over 1000 initial conditions, at $K = 1.0$, by integrating the dynamics of Eq. (1).

play an important role in synchronization in such a system. In fact, it is shown that, the transition from the unentrained phase at lower coupling strength to the entrained phase at higher coupling strength happens due to different behavior of the vortices in these two different phases. In the entrained phase, vortices are locally confined. They move in fixed paths around clusters only. However, in the unentrained phase, their motion is inconsistent and sometimes they wander off. We must note one important difference between our system and the system studied by Lee *et al.* [18]. In the previous case, the initial phases are all chosen to be zero and the vortices arise from randomness in the intrinsic frequencies. In our case, the intrinsic frequencies are identical and we study the role of randomness in the initial phase configurations. Thus, the origin of the vortices is different in these two different cases. We note that to the best of our knowledge, the underlying vortex structure for Kuramoto oscillators has not been uncovered via an explicit calculation. In the case of 2D statistical mechanics models, such as the 2D *XY* model, the underlying vortex structure can be exposed via the duality transformation [35]. We carry out the duality transformation for the Kuramoto model in the next section. We note that we start with a Hamiltonian version of the model for this.

IV. DUALITY

Recent studies show that a classical Hamiltonian system (in action-angle representation) with $2N$ state variables exhibits a family of invariant tori (on which all actions are homoge-

neous) on which the angle variables follow exactly the same dynamics as that of the Kuramoto model [33]. We use this Hamiltonian to calculate the canonical partition function to analyze the vortex and spin wave contributions of our system. We apply the duality transformation to this partition function in the next subsection.

A. Hamiltonian formulation

Consider the Hamiltonian function

$$H' = \sum_{j=1}^{N} \left\{ \frac{\omega_j}{2} \left(q_j^2 + p_j^2\right) + \frac{L}{4} \left(q_j^2 + p_j^2\right)^2 \right\}$$
$$+ \frac{1}{4} \sum_{\langle jm \rangle} K_{j,m} (q_j p_m - q_m p_j)\left(q_m^2 + p_m^2 - q_j^2 - p_j^2\right), \quad (8)$$

where ω_j, L are local parameters and $K_{j,m}$'s are symmetric coupling strengths.

Under the canonical transformation

$$I_j = \frac{\left(q_j^2 + p_j^2\right)}{2} \quad \text{and} \quad \theta_j = \tan^{-1}\left(\frac{q_j}{p_j}\right), \quad (9)$$

$j \in \{1, 2, \ldots, N\}$, the Hamiltonian takes the form

$$H(I_1, \theta_1, \ldots, I_N, \theta_N)$$
$$= \sum_{j=1}^{N} \left\{ \omega_j I_j + L I_j^2 \right\}$$
$$- \sum_{\langle jm \rangle} K_{j,m} \sqrt{I_j I_m} (I_m - I_j) \sin(\theta_m - \theta_j). \quad (10)$$

So the equation of motion in terms of the action-angle variables is

$$\dot{\theta}_j = \omega_j + 2LI_j + \sum_{\langle mj \rangle} K_{m,j} \{2\sqrt{I_m I_j} \sin(\theta_m - \theta_j)$$

$$- \sqrt{\frac{I_m}{I_j}}(I_m - I_j)\sin(\theta_m - \theta_j)\}, \tag{11}$$

$$\dot{I}_j = -\sum_{\langle mj \rangle} K_{m,j}(I_m - I_j)\sqrt{I_m I_j}\cos(\theta_m - \theta_j). \tag{12}$$

Now, for any state with homogeneous action variables $I_j = I > 0$(say), $\dot{I}_j = 0$. This means that all action variables remain invariant. For a given value of I,

$$\dot{\theta}_j = \omega_j + 2LI + \sum_{\langle mj \rangle} 2IK_{m,j}\sin(\theta_m - \theta_j)$$

$$= \tilde{\omega}_j + \sum_{\langle mj \rangle} \tilde{K}_{m,j}\sin(\theta_m - \theta_j). \tag{13}$$

Thus, this Hamiltonian function gives the evolution equations of the Kuramoto model on the invariant tori with the rescaled coupling matrix $\tilde{K}_{m,j} = 2IK_{m,j}$ and shifted frequencies $\tilde{\omega}_j = \omega_j + 2LI$.

B. Duality transformation

To start with, we consider nearest neighbor interactions and assume that all oscillators have the same intrinsic frequency and all I'_js are nearly equal. This case has also been studied in Ref. [33]. We write

$$I_m = I_{j+\mu} = I_j + \epsilon I_j + O(\epsilon^2), \tag{14}$$

where ϵ is a very small quantity. Thus,

$$\sqrt{I_m I_j} \approx I_j\left(1 + \frac{\epsilon}{2}\right) + O(\epsilon^2) \tag{15}$$

and

$$\theta_m - \theta_j = \theta_{j+\mu} - \theta_j = \Delta_\mu \theta_j.$$

Thus, the Hamiltonian takes the form

$$H = \sum_j \{\omega_j I_j + LI_j^2\} - \sum_{\langle \rangle} K\epsilon I_j^2 \sin(\Delta_\mu \theta_j). \tag{16}$$

The partition function is

$$Z = \prod_j \iint dI_j d\theta_j \exp\left[-\frac{H}{k_B T}\right]$$

$$= \prod_j \iint dI_j d\theta_j \exp\left[-\beta\{\omega_j I_j + LI_j^2\}\right]$$

$$\times \exp\left[\frac{K}{k_B T}\sum_{\langle \rangle} \epsilon I_j^2 \sin(\Delta_\mu \theta_j)\right]. \tag{17}$$

Since all actions are nearly equal, the partition function takes the form

$$Z = \prod_j \iint dI_j \delta(I_j - I)d\theta_j \exp\left[-\beta\{\omega_j I_j + LI_j^2\}\right]$$

$$\times \exp\left[\frac{K}{k_B T}\sum_{\langle \rangle} \epsilon I_j^2 \sin(\Delta_\mu \theta_j)\right] \tag{18}$$

$$= \prod_j \int d\theta_j \exp[-\beta\{\omega I + LI^2\}]$$

$$\times \exp\left[\frac{K}{k_B T}\sum_{\langle \rangle} \epsilon I^2 \sin(\Delta_\mu \theta_j)\right]. \tag{19}$$

We can choose L to be zero. Moreover, since we choose all oscillators to have identical frequencies, we can set the frequency ω to be zero without loss of generality. Hence,

$$Z = \prod_j \int d\theta_j \exp\left[\frac{K}{k_B T}\sum_{\langle \rangle} \epsilon I^2 \sin(\Delta_\mu \theta_j)\right] \tag{20}$$

$$= \prod_j \int d\theta_j \exp\left[\beta \sum_{\langle \rangle} \sin(\Delta_\mu \theta_j)\right], \tag{21}$$

where $\beta = \frac{\epsilon I^2 K}{k_B T}$. Here in our notation, μ represents the direction. This is done in the following way: We represent the phase difference between two sites i, j, say, equivalently by one of the site index j and the direction μ from j to i. Therefore,

$$\theta_i - \theta_j \equiv \theta_{j+\hat{e}_\mu} - \theta_j \equiv \Delta_\mu \theta_j, \tag{22}$$

where $\hat{e}_\mu$ is unit vector along the direction μ.

This partition function can also be written as

$$Z = \prod_j \int d\theta_j \exp\left[\beta \sum_{\langle \rangle} \cos(\Delta_\mu \theta_j + \alpha_{\mu;j})\right], \tag{23}$$

where the quantity $\alpha_{\mu;j}$ (which is $\pi/2$ in our case) is defined as a bond variable connecting lattice sites i and j, can be interpreted as a "frustration parameter." This equation maps to the partition function of the frustrated 2D XY model with nearest neighbor interactions (we discuss details of this in the Appendix). We will carry out a duality transformation [35] on the partition function with an arbitrary value α_{ij} for the frustration parameter, and in the final expression we substitute $\alpha_{\mu,j} = \pi/2$ to obtain the results for our model.

The duality transformation mentioned above, is a very useful tool in statistical physics and field theory. This transformation, under certain approximations, enables us to obtain a mapping from the low temperature phase of a given system, to the high temperature phase of the systems, and hence permits the inference of the low temperature properties of the statistical system by studying the high-temperature version and vice versa [35]. The basic idea is to rewrite the partition function in terms of the link variables on the original lattice and the constraint condition imposed by the form of the partition function on these link variables enables us to express them in terms of another set of variables, the dual variables, defined on the dual lattice sites, which is essentially the reciprocal lattice of the system [35]. For a square lattice in two-dimensions, the dual lattice is also a square lattice, which is constructed by displacing the usual lattice by half the lattice spacing in both x and y directions. Figure 9 shows an example of a square lattice in two dimensions and its dual.

We now use the relation

$$\exp\{\beta \cos \tau\} = \sum_{n=-\infty}^{+\infty} I_n(\beta)e^{in\tau}, \tag{24}$$
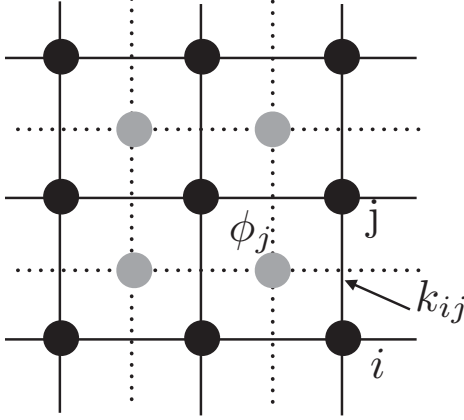
FIG. 9. This figure shows a two dimensional square lattice and its dual lattice. The original lattice is shown by black continuous lines, while the square in dotted lines represents the dual one. The k_{ij} is a link variable defined on the link connecting the sites i and j; while ϕ_j (circle in gray) is the dual variable.

where $I_n(\beta)$ is the modified Bessel function of the first kind, to rewrite the partition function as

$$
\begin{aligned}
Z &= \prod_j \int_{-\pi}^{+\pi} d\theta_j \exp\left[\beta \sum_{\langle\rangle} \cos(\Delta_\mu \theta_j + \alpha_{\mu;j})\right] \\
&= \prod_j \int_{-\pi}^{+\pi} d\theta_j \prod_{\langle\rangle} \exp[\beta \cos(\Delta_\mu \theta_j + \alpha_{\mu;j})] \\
&= \sum_{\{k_{\mu;j}\}} \prod_j \int_{-\pi}^{+\pi} d\theta_j \prod_{\langle\rangle} I_{k_{\mu;j}}(\beta) e^{ik_{\mu;j}(\Delta_\mu \theta_j + \alpha_{\mu;j})}, \quad (25)
\end{aligned}
$$

where we have introduced a set of link variables $\{k\}$ on the original lattice. Each link variable $k_{\mu;j}$ is defined on the sites at i and j (see Fig. 9) and can take only integer values. Now,

$$
Z = \sum_{\{k_{\mu;j}\}} \prod_{\langle\rangle} I_{k_{\mu;j}}(\beta) e^{ik_{\mu;j}\alpha_{\mu;j}} \prod_j \int_{-\pi}^{+\pi} d\theta_j e^{ik_{\mu;j}(\Delta_\mu \theta_j)} \quad (26)
$$

(since $I_{k_{\mu;j}}$ is independent of θ).

This can be further reduced to [35]

$$
\begin{aligned}
Z &= \sum_{\{k_{\mu;j}\}} \prod_{\langle\rangle} I_{k_{\mu;j}}(\beta) e^{ik_{\mu;j}\alpha_{\mu;j}} \prod_j \int_{-\pi}^{+\pi} d\theta_j \exp\{-i\theta_j(\Delta_\mu k_{\mu;j})\} \\
&= \sum_{\{k_{\mu;j}\}} \prod_{\langle\rangle} I_{k_{\mu;j}}(\beta) e^{ik_{\mu;j}\alpha_{\mu;j}} \prod_j \delta(\Delta_\mu k_{\mu;j}). \quad (27)
\end{aligned}
$$

This δ function constraint helps us to find the representation of $k_{\mu;j}$. The constraint enforces that $k_{\mu;j}$ are divergence-less at each lattice site. Hence, $k_{\mu;j}$ can be expressed as the curl of some new field ϕ defined at the dual lattice sites j,

$$
k_{\mu;j} = \epsilon_{\mu\nu} \Delta_\nu \phi_j. \quad (28)
$$

Thus, we can write the partition function in terms of dual space variables as

$$
\begin{aligned}
Z &= \sum_{\{\phi=-\infty\}}^{+\infty} \prod_j \exp\left(\sum_{l_d} \ln\left[I_{\epsilon_{\mu\nu}\Delta_\nu\phi_j}(\beta) e^{i(\epsilon_{\mu\nu}\Delta_\nu\phi_j)\alpha_{\mu;j}}\right]\right) \\
&= \sum_{\{\phi=-\infty\}}^{+\infty} \prod_j \exp\left(\sum_{l_d} \ln\left[I_{\epsilon_{\mu\nu}\Delta_\nu\phi_j}(\beta)\right] + i(\epsilon_{\mu\nu}\Delta_\nu\phi_j)\alpha_{\mu;j}\right),
\end{aligned}
$$
$$
(29)
$$

where the ϕ_j are now dual-space variables with the label j representing the dual-lattice sites. We now carry out the low temperature expansion of $I_n(\beta)$.

C. Low temperature expansion

We start with the integral representation of $I_n(\beta)$.

$$
\begin{aligned}
I_n(\beta) &= \frac{1}{\pi} \int_0^\pi dx e^{\beta \cos x} \cos(nx) \\
&= \sum_{p=0}^\infty \frac{(-1)^p n^{2p}}{(2p)!} \frac{1}{\pi} \int_0^\pi dx x^{2p} e^{\beta \cos x}. \quad (30)
\end{aligned}
$$

So,

$$
\begin{aligned}
\frac{I_n(\beta)}{I_0(\beta)} &= \sum_{p=0}^\infty \frac{(-1)^p n^{2p}}{(2p)!} \frac{1}{\pi I_0(\beta)} \int_0^\pi dx x^{2p} e^{\beta \cos x} \\
&= \sum_{p=0}^\infty \frac{(n^2)^p}{p!} M_p(\beta). \quad (31)
\end{aligned}
$$

Thus, we can express $I_n(\beta)/I_0(\beta)$ as a moment generating function for n^2 where the moments are

$$
M_p(\beta) = (-1)^p \frac{p!}{(2p)!} \frac{1}{\pi I_0(\beta)} \int_0^\pi dx x^{2p} e^{\beta \cos x}. \quad (32)
$$

Thus, $\ln[I_n(\beta)/I_0(\beta)]$ can be written as a cumulant generating function the pth cumulant of which would be given by

$$
C_p(\beta) = \frac{\partial^p}{\partial(n^2)^p} \ln[I_n(\beta)/I_0(\beta)]|_{n=0}. \quad (33)
$$

Using this expansion of $I_n(\beta)$ in Eq. (29) and dropping the overall multiplicative factor of $I_0^{2N}(\beta)$ (N being the system-size), we obtain [36]

$$
\begin{aligned}
Z &= \sum_{\{\phi_j=-\infty\}}^{+\infty} \exp\left(\sum_{l_d} \sum_{p=1}^\infty \frac{C_p(\beta)}{p!} (\Delta_\mu \phi_j)^{2p} + i\epsilon_{\mu\nu}(\Delta_\nu \phi_j)\alpha_{\mu;j}\right) \\
&= \sum_{\{\phi_j=-\infty\}}^{+\infty} \exp\left(\sum_{l_d} \sum_{p=1}^\infty \frac{C_p(\beta)}{p!} (\Delta_\mu \phi_j)^{2p} - i\epsilon_{\mu\nu}(\Delta_\nu \alpha_{\mu;j})\phi_j\right) \\
&= \sum_{\{\phi_j=-\infty\}}^{+\infty} \exp\left(\sum_{l_d} \sum_{p=1}^\infty \frac{C_p(\beta)}{p!} (\Delta_\mu \phi_j)^{2p} + i2\pi f_j \phi_j\right),
\end{aligned}
$$
$$
(34)
$$

where f_j is the frustration over a plaquette.

Now, using Poisson's summation identity,

$$\sum_{n=-\infty}^{+\infty} G_n = \sum_{p=-\infty}^{+\infty} \int_{-\infty}^{+\infty} dx G(x) e^{i2\pi px}. \tag{35}$$

We can write the partition function as follows:

$$Z = \sum_{\{m_j=-\infty\}}^{+\infty} \prod_j \int d\phi_j \exp\left(\sum_{l_d}\sum_{p=1}^{\infty} \frac{C_p(\beta)}{p!}(\Delta_\mu \phi_j)^{2p} + i2\pi(m_j + f_j)\phi_j\right), \tag{36}$$

where the field ϕ is now a continuum field where $-\infty < \phi < +\infty$. We also have

$$C_1(\beta) = M_1(\beta), \quad C_2(\beta) = M_2(\beta) - M_1(\beta)^2, \tag{37}$$

where $M_p(\beta)$'s are the moments. In the low temperature limit ($\beta \gg 1$), it can be shown that the main contribution comes from the series expansion of $C_p(\beta)$ up to the term β^{1-2p}. Keeping the first term alone [35] we can rewrite this partition function as

$$Z = \sum_{\{m_j=-\infty\}}^{+\infty} \int_{-\infty}^{+\infty} D\phi \exp\left(\sum_{l_d} -\frac{1}{2\beta}(\Delta_\mu \phi_j)^2 + i2\pi(m_j + f_j)\phi_j\right), \tag{38}$$

where $M_1(\beta) \approx -\frac{1}{2\beta}$ was evaluated from approximate expansion of $C_1(\beta)$. We note that the low temperature expansion series is convergent.

This functional integral over ϕ can be carried out straightforwardly and has the result

$$Z = Z^{(0)} \sum_{\{m_j=-\infty\}}^{+\infty} \exp\left[2\pi^2 \beta \sum_{i,j}(m_i + f_i)V_{ij}(m_j + f_j)\right], \tag{39}$$

where

$$V_{ij} = (\nabla^2)_{ij}^{-1}$$

is the lattice Green function in two dimension. Here the quantities $\{m\}$ can take integer values only whereas the quantities $\{f\}$ can be integer or fraction depending on the value of the frustration parameter α. For our model we have seen that, $\alpha = \frac{\pi}{2}$ which correspond to integer values of f_i. In two dimensions, the fields $\{m\}$ interact through a logarithmic potential. This expression is similar to the partition function in the low temperature regime for the 2D *XY* model with frustration. The fields are vortex excitations. We observe integer-valued vortices in our model at very low temperatures.

Thus, the duality transformation has successfully uncovered the vortices which appear in the Kuramoto model. The high temperature expansion of $I_n(\beta)$ can also yield insights into the behavior of the model which we will discuss elsewhere.

V. CONCLUSION

The relaxation dynamics of a 2D system of Kuramoto oscillators with identical frequencies coupled via nearest-neighbor coupling is investigated in detail using random initial conditions for the phases, drawn from a uniform distribution. The phase field of the oscillators of the system displays regimes with distinct characteristic features during the process of relaxation to the asymptotic states. The asymptotic states observed in the numerical simulations, which are of very long

duration, are of two distinct kinds, viz the synchronized states, and the phase locked states with vortices.

The routes for relaxation to the two kinds of asymptotic states feature characteristic structures such as synchronized clusters, vortices or topological defects, and spin waves. In the case where the final state was synchronized, the vortex-antivortex pairs annihilated each other leaving spin waves which organized themselves into a synchronized final state. For the phase locked final state, the vortex-antivortex states survive to the final asymptotic phase locked state. The basin stability of the final states was investigated. The nature of the asymptotic states was seen to be dependent on both the initial conditions as well as the system-sizes. For small system sizes, most of the initial conditions lead to complete phase-synchronized states. As system size increases, the fraction of initial conditions that lead to complete phase-synchronized states becomes small and it tends to zero in the thermodynamic limit, for the class of initial conditions studied, viz. randomly distributed phases drawn from a uniform distribution. For the large lattice sizes, the system mainly relaxes to phase-locked states which are governed by the presence of vortices or topological defects. The formation of these vortices is exposed by applying the duality transformation to the Hamiltonian version of the model.

It is interesting to note that the transition to synchronization via cluster, vortex and spin wave intermediate phases can be observed in an experimentally realisable system. Systems of magnetic spin torque oscillators are frequently studied in modern magnetism. The dynamics seen in such systems has been modelled by Kuramoto models with distance dependent coupling that falls off as d_{ij}^{-3}, where i and j are oscillator labels and d_{ij} is the Euclidean distance between them [37]. The oscillator frequencies differ from each other by a small amount. Numerical studies of such oscillators on 2D arrays show dynamics which is qualitatively similar to that observed here. Such systems should also exhibit the relaxation effects we discuss here.

We note that our initial random distribution of phases is drawn from a uniform distribution. The effect of different

distributions on the nature of the asymptotic states, and the routes to relaxation remain unexplored. Our system of oscillators also has identical frequencies. If the oscillator frequencies are drawn from a distribution, then this can also constitute a source of disorder in the system. Both these factors can introduce defects in the system. We hope to explore the interplay between these factors, and their effect on the nature of the asymptotic states and the routes to relaxation to these states in future work.

The Hamiltonian system studied over here maps onto the equilibrium *XY* model which exhibits phenomena like the topological phase transition in the form of the Kosterlitz-Thouless vortex binding-unbinding transition [38,39], despite the fact that no phase transition to long range order is expected in two-dimensions due to the Mermin-Wagner theorem [40]. The duality transformation carried out by us exposes these vortices explicitly. The perturbed Hamiltonian examined here, also contains these vortices. The duality transformation can be further exploited via the low and high temperature expansions so that the term by term contribution of the vortex configurations is exposed. Further studies via the behavior of the vortex-vortex correlation, and its behavior at low and high temperatures are possible and are planned elsewhere. For the present, we confine our numerical analysis to the vortex structures and their evolution as seen in the transient to the stationary synchronized and phase locked states.

Finally, we comment on the relation between the dynamics of the full Hamiltonian system and the Kuramoto dynamics. In the case of Hamiltonian dynamics, the over all phase space is mixed and contains sticky regions which can promote synchronisation, as well as chaotic regions and regular regions [41]. These sticky regions can have important consequences for synchronisation. Synchronization can occur in the neighbourhood of invariant curves in the phase space, where periodic trajectories can provide locally transverse stable directions. The effect of stable periodic trajectories [42], and unstable periodic trajectories [43] on synchronisation has been analysed in the case of coupled area preserving systems. The mixed nature of the phase space leads to a strong dependence on initial conditions as we see in the present case. Similar effects are seen in the study of the perturbed Hamiltonian by Witthaut *et al.* [33], where the behavior transverse to the synchronization manifold is consistent with the area preserving property. It is therefore reasonable to speculate that the Kuramoto like behavior, and the vortex effects seen here are related to mixed phase space effects seen for synchronisation in Hamiltonian systems. However, the complete confirmation of this, the study of the stability of the synchronization manifold in directions parallel and transverse to it, the role of initial conditions, and the size of the volume basin of each type of solution, requires an independent study.

APPENDIX: HAMILTONIAN FOR THE 2D *XY* MODEL WITH FRUSTRATION

The Hamiltonian for frustrated 2D *XY* model with nearest neighbor coupling is given by

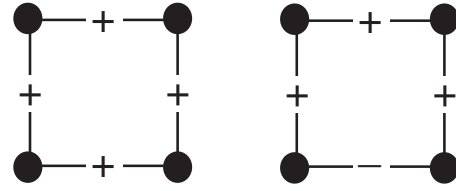$$H = -\sum_{\langle \rangle} K \cos(\theta_i - \theta_j - \alpha_{ij}). \qquad (A1)$$

FIG. 10. Left: frustration-free plaquette. Right: frustrated plaquette.

Here, the disorder is introduced in this system by adjusting the interaction in such a way that the neighboring spins at i, j get tilted by the angle α_{ij} at each bond connecting the sites i and j. Thus, generally, the ground state will no longer be ferromagnetic with all spins aligned in the same direction; instead, the direction will vary from site to site to minimize the angle difference $(\theta_i - \theta_j - \alpha_{ij})$.

In general, all bonds are satisfied in the ground state of frustration-free configurations; however, configurations with frustrations always have unsatisfied bonds and hence, in terms of energy considerations, have higher energy than the other one (Fig. 10). The frustration angle A_{ijkl} at a plaquette $ijkl$ (Fig. 11) is defined by

$$2\pi A_{ijkl} = \alpha_{ij} + \alpha_{jk} + \alpha_{kl} + \alpha_{li} \ (\text{mod} \ 2\pi). \qquad (A2)$$

Using the same notation as before, we write $\alpha_{ij} \equiv \alpha_{\mu;j}$. A plaquette can be represented by one site j and two directions μ and ν from that site. We can write the frustration field as

$$2\pi A_{\mu\nu;j} = \epsilon_{\mu\nu} \Delta_\mu \alpha_{\nu;j} = \Delta_\mu \alpha_{\nu;j} - \Delta_\nu \alpha_{\mu;j}. \qquad (A3)$$

We can associate this frustration over a plaquette to the dual site which resides at the center of the plaquette. The scalar frustration at dual site is defined as

$$f_j = \tfrac{1}{2} \epsilon_{\mu\nu} A_{\mu\nu;j}. \qquad (A4)$$

The detailed analysis of the frustrated *XY* model can be found in Ref. [44].
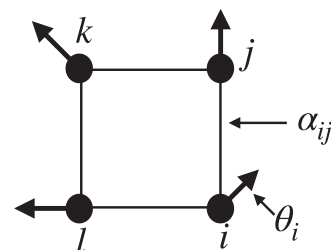

FIG. 11. One possible ground state configuration of frustrated plaquette is shown schematically. The arrows denote the orientation of spins, θ_i. The α_{ij} is the bond variable connecting the sites i and j.

[1] A. Pikovsky, J. Kurths, M. Rosenblum, and J. Kurths, *Synchronization: A Universal Concept in Nonlinear Sciences*, Vol. 12 (Cambridge University Press, Cambridge, UK, 2003).

[2] S. Strogatz, *Sync: The Emerging Science of Spontaneous Order* (Penguin, London, UK, 2004).

[3] A. T. Winfree, *The Geometry of Biological Time*, Vol. 12 (Springer, New York, 2001).

[4] K. Wiesenfeld, P. Colet, and S. H. Strogatz, Phys. Rev. Lett. **76**, 404 (1996).

[5] M. Silber, L. Fabiny, and K. Wiesenfeld, JOSA B **10**, 1121 (1993).

[6] D. J. DeShazer, R. Breban, E. Ott, and R. Roy, Phys. Rev. Lett. **87**, 044101 (2001).

[7] Y. Kuramoto, in *International Symposium on Mathematical Problems in Theoretical Physics*, Lecture Notes in Physics Vol. 30, edited by H. Araki (Springer, New York, 1975), p. 420.

[8] Y. Kuramoto, Prog. Theor. Phys. **76**, 576 (1986).

[9] S. H. Strogatz, Physica D **143**, 1 (2000).

[10] H. Hong, H. Chaté, H. Park, and L.-H. Tang, Phys. Rev. Lett. **99**, 184101 (2007).

[11] H. Sakaguchi, S. Shinomoto, and Y. Kuramoto, Prog. Theor. Phys. **77**, 1005 (1987).

[12] S. H. Strogatz and R. E. Mirollo, Physica D **31**, 143 (1988).

[13] T. Aoyagi and Y. Kuramoto, Phys. Lett. A **155**, 410 (1991).

[14] M. Bahiana and M. S. O. Massunaga, Phys. Rev. E **49**, R3558(R) (1994).

[15] J. L. Rogers and L. T. Wille, Phys. Rev. E **54**, R2193 (1996).

[16] M. Maródi, F. d'Ovidio, and T. Vicsek, Phys. Rev. E **66**, 011109 (2002).

[17] H. Hong, H. Park, and M. Y. Choi, Phys. Rev. E **72**, 036217 (2005).

[18] T. E. Lee, H. Tam, G. Refael, J. L. Rogers, and M. C. Cross, Phys. Rev. E **82**, 036202 (2010).

[19] H. Daido, Prog. Theor. Phys. **77**, 622 (1987).

[20] H. Daido, Phys. Rev. Lett. **68**, 1073 (1992).

[21] M. C. Cross and P. C. Hohenberg, Rev. Mod. Phys. **65**, 851 (1993).

[22] S.-Y. Ha, D. Ko, and Y. Zhang, SIAM J. Appl. Dyn. Syst. **17**, 581 (2018).

[23] M. K. Stephen Yeung and S. H. Strogatz, Phys. Rev. Lett. **82**, 648 (1999).

[24] H. Wu and M. Dhamala, Phys. Rev. E **98**, 032221 (2018).

[25] F. Dai, S. Zhou, T. Peron, W. Lin, and P. Ji, Phys. Rev. E **98**, 052218 (2018).

[26] H. Hong, H. Park, and L.-H. Tang, Phys. Rev. E **76**, 066104 (2007).

[27] P. Ji, T. K. Peron, F. A. Rodrigues, and J. Kurths, Sci. Rep. **4**, 4783 (2014).

[28] J. Um, H. Hong, and H. Park, Phys. Rev. E **89**, 012810 (2014).

[29] S.-W. Son, H. Jeong, and H. Hong, Phys. Rev. E **78**, 016106 (2008).

[30] H. Daido, Phys. Rev. E **61**, 2145 (2000).

[31] A. Ghosh and S. Gupta, Physica A **392**, 3812 (2013).

[32] H. Daido, Chaos **28**, 045102 (2018).

[33] D. Witthaut and M. Timme, Phys. Rev. E **90**, 032917 (2014).

[34] B. J. Kim, M. Y. Choi, S. Ryu, and D. Stroud, Phys. Rev. B **56**, 6007 (1997).

[35] R. Savit, Rev. Mod. Phys. **52**, 453 (1980).

[36] R. Savit, Phys. Rev. B **17**, 1340 (1978).

[37] V. Flovik, F. Macia, and E. Wahlström, Sci. Rep. **6**, 32528 (2016).

[38] J. M. Kosterlitz and D. J. Thouless, J. Phys. C **6**, 1181 (1973).

[39] J. Kosterlitz, J. Phys. C **7**, 1046 (1974).

[40] N. D. Mermin and H. Wagner, Phys. Rev. Lett. **17**, 1133 (1966).

[41] G. Zaslavsky, Physica D **168**, 292 (2002).

[42] S. Mahata, S. Das, and N. Gupte, Phys. Rev. E **93**, 062212 (2016).

[43] J. F. Heagy, T. L. Carroll, and L. M. Pecora, Phys. Rev. E **52**, R1253(R) (1995).

[44] S. Teitel and C. Jayaprakash, Phys. Rev. B **27**, 598 (1983).